Nano and Medical Materials 2022, 2(1), 40.
https://doi.org/10.59400/nmm.v2i1.40

Article

Dopamine and antioxidant grape seed extract loaded chitosan nanoparticles: A preliminary in vitro characterization

Stefano Bellucci[1,*], Giuseppe Fracchiolla[2,*], Alessandra Pannunzio[2], Antonello Caponio[2], Daniela Donghia[2], Filomena Corbo[2], Loredana Capobianco[3], Antonella Muscella[3], Daniela Erminia Manno[4], Erika Stefàno[3], Santo Marsigliante[3], Adriana Trapani[2]

[1] National Institute of Nuclear Physics-National Laboratories of Frascati, I-00044 Rome, Italy
[2] Department of Pharmacy-Drug Sciences, University of Bari "Aldo Moro", 70125 Bari, Italy
[3] Department of Biological and Environmental Sciences and Technologies, University of Salento, I-73100 Lecce, Italy
[4] Department of Mathematics and Physics "E. De Giorgi", University of Salento, 73100 Lecce, Italy
*** Corresponding authors:** Stefano Bellucci, stefano.bellucci@lnf.infn.it; Giuseppe Fracchiolla, giuseppe.fracchiolla@uniba.it

CITATION

Bellucci S, Fracchiolla G, Pannunzio A, et al. Dopamine and antioxidant grape seed extract loaded chitosan nanoparticles: A preliminary in vitro characterization. Nano and Medical Materials. 2022; 2(1): 40. https://doi.org/10.59400/nmm.v2i1.40

ARTICLE INFO

Received: 14 April 2022
Accepted: 13 May 2022
Available online: 20 May 2022

Abstract: Neuronal cell model line SHSY-5Y is extensively adopted when in vitro investigations are related to Parkinson disease (PD) application. Herein, chitosan nanoparticles (CS NPs) were formulated for the co-administration of dopamine (DA) and grape seed extract (GSE) with the aim to gain insight into the interactions occurring between SHSY-5Y and NPs. Following the ionic gelation technique, the mean particle size of the NPs resulted in the range 310–330 nm and the zeta measurements were in the range +16.4–+35.5 mV. The presence of CS chains on the surface suggested by positive zeta values was also confirmed by FT-IR analysis, whereas storage stability studies upon different temperatures evidenced that, although aggregation occurred, DA autoxidation was prevented because no black suspensions were detected over the time, irrespectively of the temperature assayed. From a biological viewpoint, release studies of CS NPs loaded with DA and GSE showed that in SHSY-5Y cell lines DA accumulation was time-dependent, irrespectively of the presence of GSE. Furthermore, ROS levels and carbonylated proteins both decreased in SHSY-5Y cell line once NPs administering both DA and GSE were incubated, suggesting a significative reduction of oxidative stress which plays a significative role for PD development.

Keywords: dopamine; chitosan nanoparticles; radical oxygen species; SHSY-5Y cell line; OxyBlot analysis

1. Introduction

Among biopolymers for drug delivery purposes, the polysaccharide chitosan (CS) is extensively used because of its favorable features, including mucoadhesion, biocompatibility and the ability to transiently open the tight junctions of the epithelial layers [1,2]. For instance, since 1990's, chitosan nanoparticles (CS NPs) have paid attention to the mild method of ionic gelation occurring in their preparation, which allows several applications in humans, including the use of different routes of administration [3–5]. The final properties of the NPs can be modulated by the molecular weight of the adopted CS and its deacetylation degree, also allowing to different active substances to be loaded and addressed to the targeting site. From a clinical viewpoint, in the case of antioxidant agents' delivery, the needing of their supply to the Central Nervous System is relevant because such compounds can contribute to ameliorate patients affected by neurodegenerative

disorders such as Parkinson disease (PD). For such pathology, the mechanisms of "mitochondrial dysfunction and oxidative stress" and the "neuroinflammation" are well known to be involved in its pathogenesis together with the needing to supply the neurotransmitter dopamine (DA) whose low levels are essential in the Substantia Nigra [6,7]. Hence, beneficial effects of antioxidant molecules are expected once they are administered as such or in combination with anti-compounds. In this regard, several examples of CS NPs for the vectorization of polyphenol-based antioxidant compounds have been reported in the literature [8–12]. For instance, narigenine and ellagic acid were recently loaded in CS NPs and tested for their protective effects in neuronal cell lines, as a prediction of their anti-PD activity [10,11]. Among polyphenols arising from natural sources, grape seed extract (GSE) is a mixture where pro-antocyanidines are predominant and its importance for PD treatment has been previously shown [13]. Moreover, GSE incorporation in NPs made of a CS derivative was already attempted with the scope to increase the resistance of endothelial progenitor cells to oxidative stress, but to the best of our knowledge, CS NPs containing both GSE and DA applied for PD treatment have never been described [12]. Therefore, herein we have investigated CS NPs where two active principles were co-loaded, namely, DA and GSE, with the aim to gain insight into some biochemical changes in terms of radical oxygen species (ROS) production, the amounts of carbonylated proteins induced by such NPs in the neuronal SHSY-5Y cells. Indeed, CS and CS derivatives NPs administering DA alone were previously studied by us, adopting high molecular weight CS for the formulation instead of the low molecular weight CS herein selected with the idea in mind to explore a different type of polycation for NP production [1,5,14]. On the other hand, another colloidal carrier represented by solid lipid nanoparticles (SLNs) was recently investigated by us for the feasibility to load GSE alone or also in the presence of DA in view of PD application [13,15,16]. Overall, in the present work, the in vitro studies focusing on the hydrophilic carrier represented by CS NPs instead of hydrophobic SLNs allowed us to obtain preliminary information for an alternative delivery system able to vectorize both DA and GSE.

2. Experimental method

2.1. Materials

Chitosan hydrochloride was purchased from Heppe Medical Chitosan GmbH (Halle, Germany). According to the manufacturer's instructions, the mean molecular weight was in the range 60–80 KDa. DA hydrochloride, KBr, Tween 20, dimethylsulphoxide, pentasodium tripolyphosphate (TPP) heat-inactivated fetal bovine serum (FBS), penicillin, streptomycin and glutamine were purchased from Sigma–Aldrich (Milan, Italy). grape seed extract containing ≥ 95.0% of proanthocyanidins was bought from Farmalabor (Canosa di Puglia, Italy). All other chemicals were reagent grade. Ultrapure water was used throughout the study.

2.2. NP formulation

The preparation of DA/CS NPs was carried out following the ionic gelation

method [5]. A 0.2% w/v solution of CS was prepared in aqueous solution of diluted acetic acid (0.1% v/v). Then, DA was dissolved in the polysaccharide solution to achieve the final concentration of 0.5% w/v. To 0.75 ml of the resulting CS solution, 0.2 mL of an aqueous solution of TPP (0.07%, w/v) were pipetted to induce NP formation under moderate magnetic stirring (20 rpm, Securlab, Rome, Italy) at room temperature under light protection. The resulting NPs were centrifuged (16,000 × g, 45 min, Eppendorf 5415D, Hamburg, Germany), the supernatant was addressed to DA/GSE quantification via HPLC analysis and the obtained pellet was resuspended in distilled water for further studies. The so-obtained NPs were indicated as "CS DA TPP NPs".

To adsorb GSE onto the NP surface separately, an aqueous solution of 0.1% w/v of GSE was prepared. To 1 mL of GSE solution, 0.5 mL of CS DA TPP nanosuspensions previously obtained as above were added and for 3 hours under light protection at room temperature were let to incubate to promote physical adsorption. Afterwards, centrifugation (16,000 × g, 45 min, Eppendorf 5415D, Hamburg, Germany) was performed in order to isolate colloidal particles. The resulting NPs were herein indicated as "CS DA TPP NPs ads GSE". In the absence of DA and in the absence of adsorption, the NPs were taken as control and indicated as "CS TPP NPs". The NPs prepared as above in the absence of DA but adsorbed GSE were called "CS TPP NPs ads GSE".

2.3. Physico-chemical characterization of NPs

A Zetasizer Nano ZS (ZEN 3600, Malvern, UK) equipment following the photon correlation spectroscopy (PCS) mode allowed measurements of size and polydispersion index (PDI) of NP formulations. Precisely, particle size and PDI were measured after NP dilution 1:1 (v:v) with double distilled water, while the zeta potential value was determined after NP dilution 1:20 (v:v) in the presence of KCl (1 mM, pH 7) [17,18].

A Hitachi 7700 electron microscope in cryogenic mode was used to analyze the morphology and size of CS DA TPP NPs and CS DA TPP NPs ads GSE. All observations were carried out at an accelerating voltage of 100 kV and a temperature of 105 K. The samples were vitrified according to the previously described procedure [19]. Briefly, a drop of the suspension containing the NPs was deposited on carbon-coated grids and, after removing the excess solution with filter paper, NPs were vitrified by immersion in liquid ethane, kept just above the freezing point, and finally transferred onto the Gatan 626 cryo support. An AMT-XR-81 camera was used to acquire the digital images. The morphology and size of the particles were determined by processing twenty randomly selected fields at different magnifications, by adopting 500 counts per sample.

DA and GSE quantifications were carried out by HPLC as previously reported and under such chromatographic conditions, the retention times of DA and GSE were found to be equal to 5.5 min and 12 min, respectively. For DA calibration, curve linearity ($R^2 > 0.999$) was checked over the range of concentrations tested (4.75×10^{-4} to 1.5×10^{-5} M), whereas for GSE calibration curve linearity ($R^m > 0.999$), the range of concentrations was found to be 100–50 mg/mL [13].

To determine the encapsulation efficiency (E.E.) referring to DA and GSE in the

obtained NPs, the samples underwent to centrifugation as described in section 2.2 and the resulting supernatants were then analyzed by HPLC for DA (or GSE) content. The E.E.% was calculated as follows (Equation (1)):

$$\text{E.E.\%} = \text{Total DA (or GSE)} - \text{DA (or GSE) in the supernatant after centrifugation/Total DA (or GSE)} \times 100 \quad (1)$$

where total DA (or total GSE) is the starting amount of DA (or GSE) used for NP production. Each measurement was performed in triplicate.

Moreover, for NPs, pH values were measured at 25 °C by a FiveEasy pH meter apparatus (Levanchimica, Bari, Italy).

2.4. Size stability studies

For both CS DA TPP NPs and CS DA TPP NPs ads GSE physical stability was evaluated by measuring particle size during incubation upon the following conditions of storage: i) 4 °C for 3 weeks; ii) 25 °C for 1 week; iii) 37 °C for 24 h [20]. For each temperature of storage, the particle size was measured at appropriate time points, following the PCS methodology described in Section 2.3. For each temperature of storage, the study was carried out in triplicate.

2.5. FT-IR spectroscopy

Powders of 2–5 mg of freeze-dried CS TPP NPs, CS DA TPP NPs, CS TPP NPs ads GSE NPs and CS DA TPP NPs ads GSE NPs (Lio Pascal 5P, Milan, Italy) were milled into KBr discs prior to acquiring FT-IR spectra on a Perkin Elmer 1600 FT-IR spectrometer (Perkin Elmer, Milan Italy). FT-IR spectra were also acquired for pure CS, DA, and GSE. The spectroscopic analysis was performed at room temperature (range: 4000–400 cm^{-1}; resolution: 1 cm^{-1}) [21,22].

2.6. Cell cultures

SHSY-5Y cell line were cultivated in DMEM medium (Sigma, St. Louis, MO, USA) supplemented with 10% FBS, glutamine, 2 mM penicillin (100 I.U./mL) and streptomycin (100 mg/mL). A humidified incubator set 37 °C and containing 5% CO_2 in air was used for cell cultivation.

2.7. Cytotoxicity assay

The inhibition of SHSY-5Y cell proliferation was investigated according to sulforhodamine B (SRB) assay. For this assay, cells at 70–80% confluency were exposed to trypsin (0.25% trypsin with 1 mM EDTA), washed, and resuspended in growth medium; then, 100 µL of a cell suspension (10^5 cells/mL) were added to each well of a 96-well plate and an overnight incubation was planned. Afterwards, cells were treated with different concentrations of CS TPP NPs ads GSE (0–0.8 µg/mL), CS DA TPP NPs ads GSE and DA (0–50 µg/mL) for 24 and 48 h. After treatment, 10% trichloroacetic acid (TCA) and 0.4% (w/v) SRB dissolved in 1% acetic acid allowed SHSY-5Y cell fixation. SRB was removed and the plates washed four times with 1% acetic acid in order to discard unbound dye before air-drying. Bound SRB was then dissolved in 200 µL of 10 mM unbuffered Tris-based solution and the

plates were left on a plate shaker for at least 10 min. Absorbance was measured in a 96-well plate reader at the wavelength of 492 nm via the use of a SpectroStar spectrophotometer (BMG Labtech, Ortenberg, Germany). The percentage cell survival was calculated as the absorbance ratio of treated to untreated cells. The data shown are means ± standard deviation (S.D.) arising from eight replicates of five independent experiments.

2.8. ROS determination

ROS generation was evidenced according to the colorimetric nitro blue tetrazolium (NBT, Thermo Fisher Scientific, Milan, Italy) assay, based on the reduction of yellow water-soluble tetrazolium chloride by superoxide to an insoluble violet formazan [23,24]. SHSY-5Y cells were exposed to DA (10 μg/mL), CS DA TPP NPs ads GSE (DA set at 10 μg/mL), and CS TPP NPs ads GSE (GSE set at 0.15 μg/mL) for different time points (ranging from 5 min to 24 h). After treatment, the culture medium was replaced with unconditioned medium enriched with NBT (1 mg/mL) at 37 °C for 1 h. Then, cells were washed and lysed in a 90% dimethylsulphoxide solution containing 0.01 N NaOH and 0.1% SDS. Absorbance of formazan was measured at the wavelength of 620 nm (BMG Labtech, Ortenberg, Germany) and data were plotted as % of control untreated cells.

2.9. In vitro DA/GSE release studies

SH-SY5Y cells were treated at 80% confluence with CS DA TPP NPs (DA = 20 μg/mL) or with CS DA TPP NPs, ads GSE (0.07 μg/mL) for 1, 6 and 24 h and pure GSE (0.07 μg/mL) for 1, 6 and 24 h. The culture medium was replaced with fresh medium 24 h prior to experiments. After treatment, cells were washed twice in ice-cold PBS and collected in RIPA lysis buffer (Merk KGaA, Darmstadt, Germany) supplemented with the inhibitor cocktail, protease, containing AEBSF, Aprotinin, Bestatin, E-64, Leupeptin, Pepstatin A (Merk KGaA, Darmstadt, Germany) and NaF (1 mM). Then, aliquots of 100 μL were withdrawn and added to 900 μL of cold acetonitrile in order to deproteinize the samples arising from the lysis [25]. After mixing and centrifugation (16,000 g, 45 min, Eppendorf 5415D, Hamburg, Germany), the resulting clear supernatant was analyzed by HPLC as above described for the amounts of DA and GSE released.

2.10. OxyBlot assay

The effects of DA, CS TPP NPs ads GSE and CS DA TPP NPs ads GSE, on the oxydation of cellular proteins were measured by OxyBlot assay using OxyBlotTM Protein Oxidation Detection Kit (S7150; Chemicon, Temecula, CA, US).

Proteins derived from each sample with an equal amount were divided into two aliquots. After the denaturation of each sample with 6% SDS (w/v), one aliquot was derivatized with 2,4-Dinitrophenylhydrazine (DNPH) solution; the other aliquot was reacted with derivatization-control solution to serve as a non-derivatized control. Thereafter, the derivatized and non-derivatized proteins were resolved by 12% SDS-PAGE and then transferred onto a nitrocellulose membrane.

After blocking of nonspecific binding, the membrane was incubated with rabbit

polyclonal anti-dinitrophenyl primary antibody at a dilution of 1:150 in Tris-buffered saline (TBS), 0.1% Tween-20, 5%, at room temperature for 1 h. After washing, the membrane was further incubated with Goat Anti-Rabbit IgG (HRP-conjugated) secondary antibody at a dilution of 1:300 in TBS 0.1% Tween-20.5%, at room temperature for 1 h. The immunoreactive protein bands were then visualized by ECL chemiluminescence substrate and the ChemiDoc Imaging System (Bio-Rad, Hercules, CA, US).

Intensities of oxidized protein bands in each lane were measured by Image Lab software (version 6.1 Bio-Rad, Hercules, CA, US).

2.11. Statistics

For physico-chemical properties and size stability studies, statistical analyses were carried out using Prism Version 4, GraphPad Software Inc. (San Diego, CA, USA). Data were expressed as either mean ± SD. Multiple comparisons were based on one-way analysis of variance (ANOVA) with either Bonferroni's or Tukey's post hoc test, and differences were considered significant when $p < 0.05$.

For biological studies, experimental points represented means ± SD of three to five independent experiments, performed in eight replicates, undergoing statistical evaluation using the ANOVA test. Where shown in the Figures, post hoc tests (Bonferroni/Dunn) were also performed to reinforce statistical evaluation.

3. Results

3.1. Physico-chemical characterization of NPs

Table 1 deals with the main physico-chemical characterization of NPs under investigation. The smallest particles were the unloaded CS TPP NPs with a mean diameter equal to 179 ± 10 nm, whereas the addition of the neurotransmitter alone and, afterwards, the physical adsorption of GSE induced size enlargement, resulting in NPs whose particle mean diameter was in the range 310–330 nm. As shown in **Table 1**, due to the physical GSE, adsorption size distribution was broad, as demonstrated by the higher values of PDI (0.45–0.55 and 0.40–0.50 for CS TPP NPs ads GSE and CS DA TPP NPs ads GSE, respectively). **Figures 1c,d** show TEM images from CS DA TPP NPs and TEM images of NPs from CS, DA, TPP, ads GSE, respectively.

As evident from the wide field, the nanoparticles have a spherical shape and very similar size. For each sample, the diameter of the NPs was measured and the results were statistically processed (see histograms in **Figures 1c,d**). The radius (R) distribution was fitted with a Gaussian function. For the CS DA TPP NPs, a monodisperse distribution was obtained with main value $R = 105$ nm and a standard deviation of 30 nm. The CS, DA, TPP, NPs, ads GSE show a broader bimodal beam distribution and the principal values determined are $R1 = 70$ nm and standard deviation 30 nm, and $R = 115$ nm and standard deviation 40 nm.

Concerning the zeta potential values, for all formulations investigated, positive values were detected in good agreement with the exposure of CS chains outside the NPs. Moreover, CS TPP NPs ads GSE exhibiting a zeta potential value equal to

+24.0 mV (** $p \leq 0.001$), induced to suppose that, as expected, the physical adsorption of GSE led to an external localization of the antioxidant mixture. Regarding E.E. for DA, high values were obtained (49 ± 7–50 ± 6), both in the presence or in the absence of GSE adsorption (**Table 1**). When all tested nanosuspensions underwent to pH measurements, acidic values were achieved in the range 3.30–4.10, according to the fact that the CS dissolving medium was represented by diluted acetic acid.

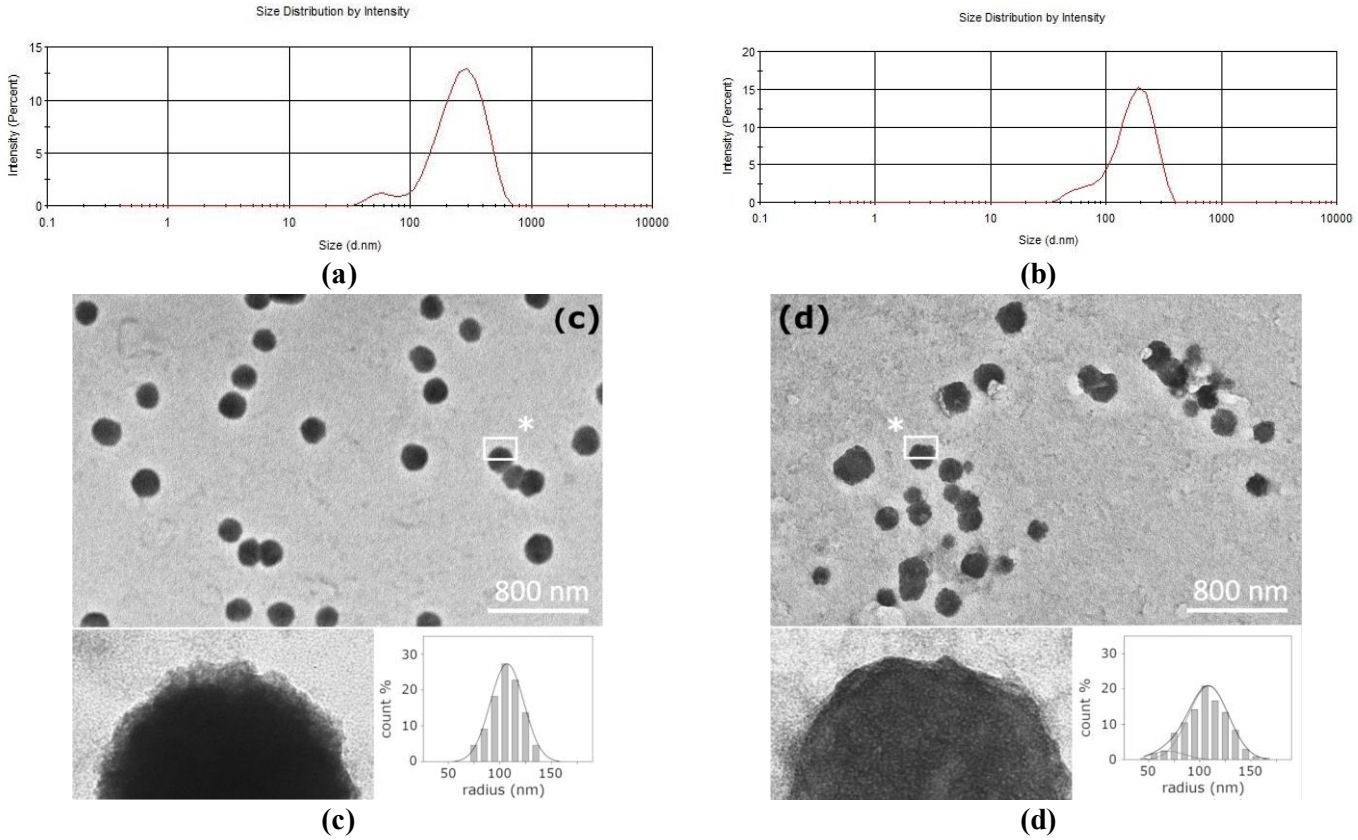

Figure 1. (a) Particle size distribution of NPs, CSDA, TPP; **(b)** NPs, CSDA, TPP, ads GSE; **(c)** TEM images of CS, DA, TPP, NPs; **(d)** CS DA TPP NPs ads GSE.

Table 1. Physicochemical properties of DA (with or without GSE) containing NPs. Mean ± S.D. are reported, $n = 6$. CS TPP NPs were used as control for statistical evaluation. (*) $p \leq 0.01$; (**) $p \leq 0.001$.

Formulation	Size (nm)	PDI	Zeta potential (mV)	E.E. DA (%)	E.E. GSE (%)	pH
CS TPP NPs	179 (± 10)	0.42–0.44	+30.4 (± 0.7)	–	–	3.75 (± 0.03)
CS DA TPP NPs	310 (± 33)**	0.40–0.41	+16.4 (± 1.7)**	50 (± 6)	–	3.30 (± 0.09)
CS TPP NPs ads GSE	330 (± 5)**	0.45–0.55	+24.0 (± 2.9)**	–	19 (± 1)	4.10 (± 0.04)
CS DA TPP NPs ads GSE	326 (± 9)**	0.40–0.50	+35.5 (± 2.6)*	49 (± 7)	28 (± 4)	3.65 (± 0.1)

3.2. Physical stability of NPs

The physical stability of NPs was compared between CS DA TPP NPs and CS DA TPP ads GSE NPs, by measuring the particle size of such formulations after storage at 4 °C for 3 weeks or at 25 °C for 1 week as well as for 24 h at 37 °C (**Figure 2a,b,c**). In detail, storage at 4 °C could be prolonged up to 21 days only for

CS DA TPP NPs with a marked particle size increase over time (** $p \leq 0.001$, **Figure 2a**). On the other hand, aggregates already occurred when CS DA TPP ads GSE NPs were stored over 14 days at 4 °C (**Figure 2a**). By increasing the temperature of storage, as it could be seen in **Figure 2b,c** referring to 25 °C and 37 °C, respectively, CS DA TPP NPs underwent to faster aggregation, reaching micron-sized particles. CS DA TPP NPs ads GSE provided bigger particle size than CS DA TPP NPs at 25 °C rather than at 37 °C. Precisely, at 25 °C aggregates of CS DA TPP NPs ads GSE appeared at 4 days of incubation vs 7 days of CS DA TPP NPs with significant statistical differences in comparison to the initial particle size of each formulation (**Figure 2b**). Moreover, at 37 °C aggregates of CS DA TPP NPs ads GSE were detected at 24 h vs 17 h of CS DA TPP NPs and, for the former NPs, a marked particle size enlargement was revealed starting from 1 h (** $p \leq 0.001$) instead of at the latest time points (**Figure 2c**). Overall, through the study of physical stability, although aggregates were detected, no black precipitates were seen, suggesting that NPs were able to protect DA from early autoxidation.

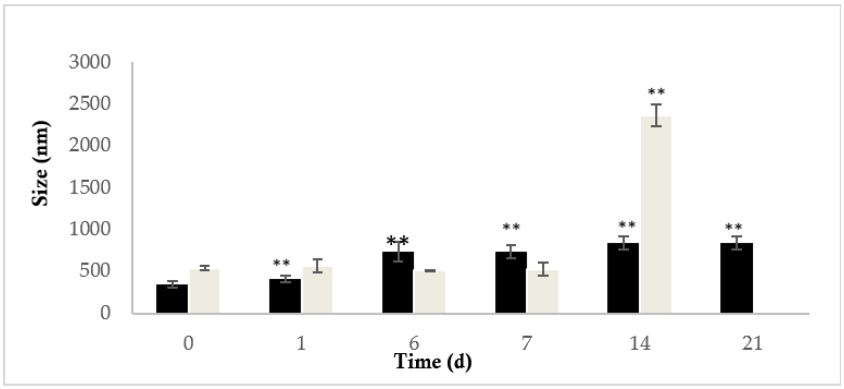

(a)

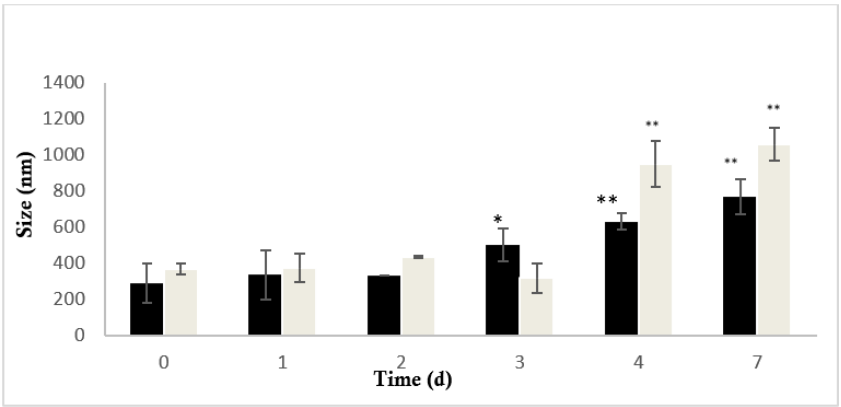

(b)

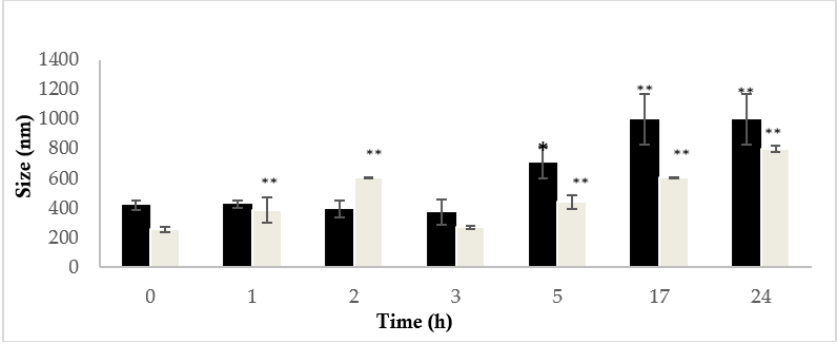

(c)

Figure 2. Physical stability of CS DA TPP NPs (black bars) and CS DA TPP NPs ads GSE (grey bars) under three different temperatures of storage. **(a)** 4 °C; **(b)** 25 °C; **(c)** 37 °C. For each temperature, the particle size at time zero was the reference control value. (*) $p \leq 0.01$; (**) $p \leq 0.001$.

3.3. FT-IR studies

The solid state of NPs under investigation was characterized by recording FT-IR spectra which are shown in **Figure 3a,b**. The typical crystalline state of the pure substances DA and GSE was derived from the corresponding FT-IR spectra shown in **Figure 3b**, curves a), b), but, once the FT-IR spectra of the NPs were considered, an amorphous state of DA and/or GSE was evidenced (**Figure 3a**, (curve d)); **Figure 3b**, (curves c), d)). The typical stretching band of C=O of pure CS at 1645 cm^{-1} was shifted at 1638 cm^{-1} in the FT-IR spectrum of CS TPP NPs (**Figure 3a**, curve c)), confirming the external position of the polycation outside such NPs. For CS DA TPP NPs ads GSE (**Figure 3b**, (curve d)), the characteristic peaks attributable to pure DA and pure GSE at 1616–1579 cm^{-1} and at 1609 cm^{-1}, respectively, were not distinctly detected but the stretching band of C=O at 1635 cm^{-1} could be again attributed to the CS presence on the external side of the NPs.

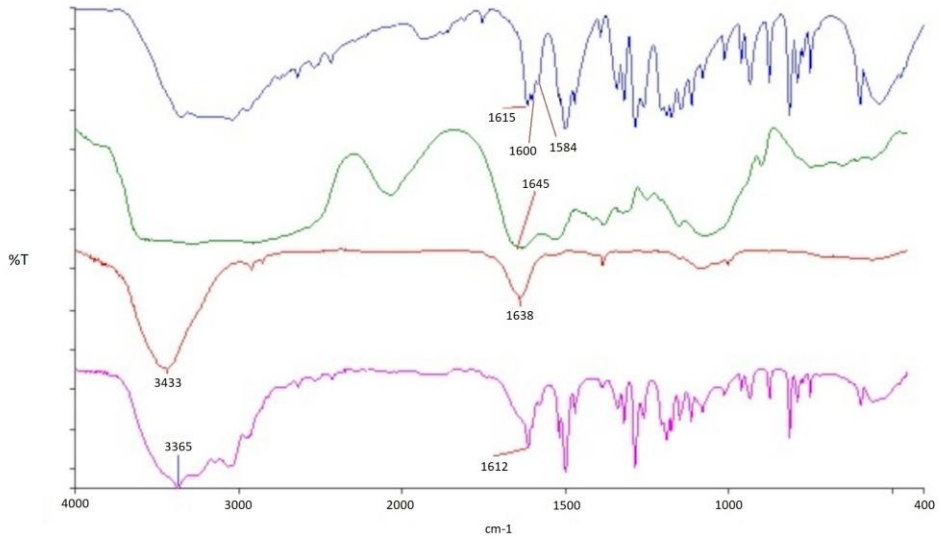

(a)

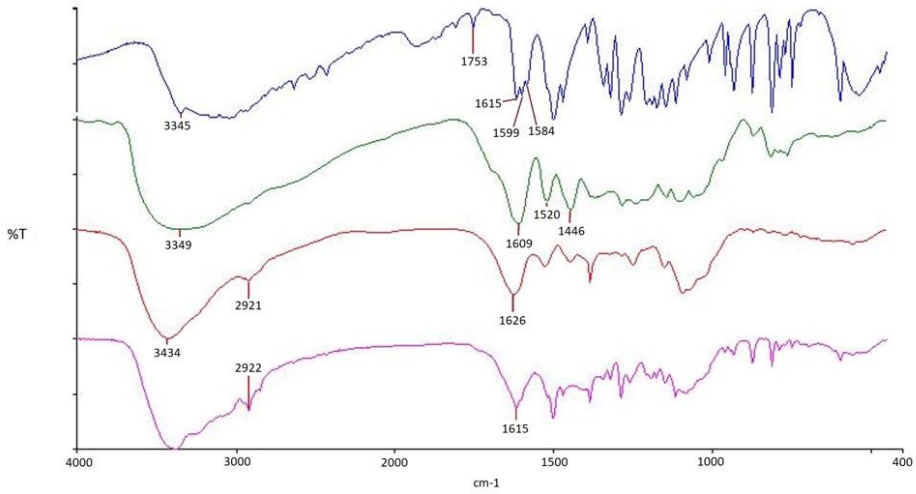

(b)

Figure 3. (a) FT-IR spectra of pure DA a); pure CS b); CS TPP NPs c) and CS DA TPP NPs d); **(b)** FT-IR spectra of pure DA a); pure GSE b); NPs CS TPP ads GSE c) and CS DA TPP NPs ads GSE d).

3.4. Cell viability

As already seen, DA reduced SHSY-5Y cell viability in a dose-dependent (1–50 μM) manner (**Figure 4a**). On the other hand, CS TPP NPs ads GSE completely reversed the effect on cell vitality of DA, and such NPs did not alter SHSY-5Y cell viability, at both 24 h and 48 h as times of incubation, irrespectively of the concentration used (**Figure 4a**).

3.5. ROS production

In this study, the effect of CS DA TPP NPs ads GSE on ROS generation in SHSY-5Y cells was investigated. As shown in **Figure 4b**, exposure of SHSY-5Y cells to 10 μg/mL DA led to a 2.1-fold increase compared with the control, whereas CS DA TPP NPs ads GSE significantly inhibited the increase in intracellular ROS production in SHSY-5Y cells. Notably, incubation with 0.15 μg/mL of CS TPP NPs ads GSE alone did not cause any ROS production in the SHSY-5Y cells (**Figure 4b**).

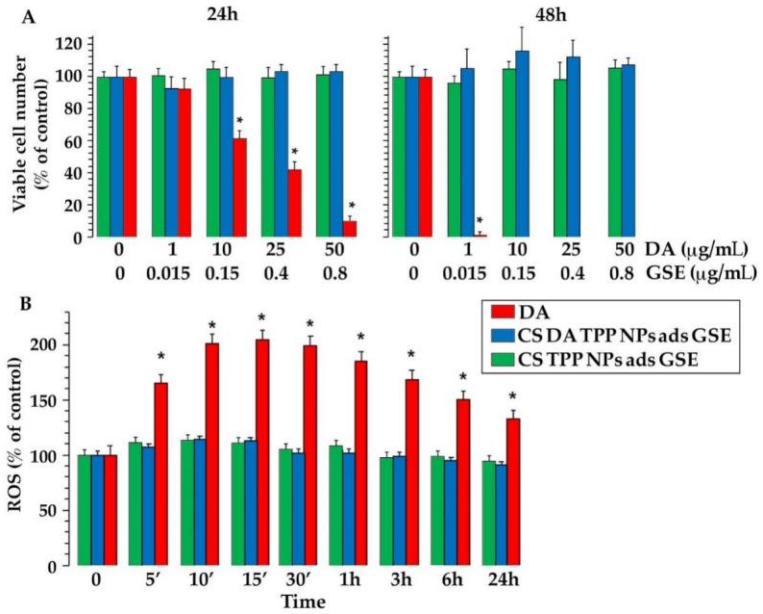

Figure 4. Biological effects of CS DA TPP NPs, ads GSE on SHSY-5Y cells. A. Sensitivity of SHSY-5Y cells to CS DA TPP, NPs ads GSE. Cells were treated with and without increasing concentrations of DA, CS DA TPP NPs ads GSE, CS TPP NPs ads GSE and viable cell number was determined 24 h or 48 h later with SRB assay. The data are means ± S.D. of four different experiments run in eight replicates and are presented as percent of control. B. ROS generation was detected by colorimetric NBT assay. The data are means ± S.D. obtained from three independent experiments performed with eight replicates in each and are presented as a percentage of control. Asterisks indicate values that are significantly different between DA and CS TPP NPs ads GSE at the same GSE concentration (Student's *t*-test, * $p < 0.05$).

3.6. DA/GSE release in SHSY-5Y cell line

Total intracellular DA content was evaluated in SH-SY5Y after treatment with 20 µg/mL DA loaded in CS TPP NPs as GSE or in CS TPP NPs after 1, 6, and 24 h of incubation. Interestingly, DA cellular accumulation was found to be time dependent, although 3–4 times less when CS DA TPP NPs and GSE were incubated in comparison to CS DA TPP NPs (**Figure 5**). On the other hand, pure GSE was found quantitatively inside the cells within 24 h (**Figure 5**).

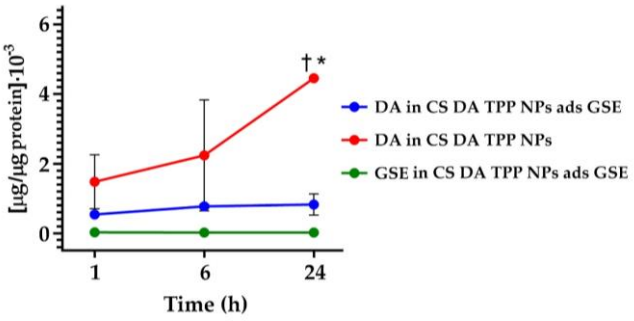

DA released in SH-SY5Y		
Time	CS DA TPP NPs ads GSE	CS DA TPP NPs
1h	8.81%	32.63%
6h	10.58%	33.65%
24h	16.59%	47.22%

Figure 5. Intracellular DA concentration after CS DA TPP NPs ads GSE or CS DA TPP NPs (25 µg/mL DA) treatments in SH-SY5Y cell lines. The intracellular DA concentration was determined by HPLC; cells were continuously exposed to the compounds for 1, 6, or 12 h. Each point represents the means ± S.D. of three different experiments and is indicated as µg (referred to as DA or GSE only when alone)/µg of protein. * Indicates values that are significantly different (* $p < 0.05$, values that are significantly different at the same time point; † $p < 0.05$, values that are significantly different between 1 h and 24 h points).

3.7. OxyBlot analysis

We determined the effects of DA and NPs administering DA and GSE on the oxidation of cellular proteins by OxyBlot analysis. The significant accumulation of oxidatively modified proteins in SHSY-5Y neuroblastoma cells ($p < 0.0001$) clearly indicates the pro-oxidant activity of DA (25 µg/mL, **Figure 6**). On the other hand, a smaller amount of carbonylated proteins levels (carbonylated proteins/b-actin ratio ≤ 1) was observed in SHSY-5Y neuroblastoma cells treated with CS DA TPP NPs ads GSE and CS TPP NPs ads GSE (**Figure 6**).

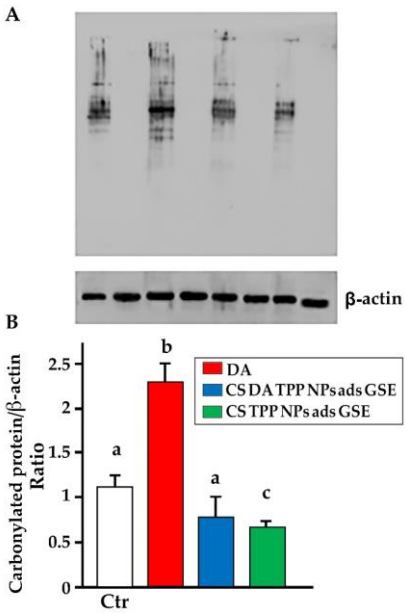

Figure 6. Carbonylation of intracellular proteins. A. Detection of oxidized proteins in cell lysates isolated from SHSY-5Y neuroblastoma cells. Cells were treated for 15 min with DA (25 μg/mL), CS TPP NPs ads GSE and CS DA TPP NPs ads GSE, and the oxidation of cellular proteins was measured by OxyBlot assay. Anti *β*-actin antibody was used to verify equal loading of cell lysate samples (lower panel). Blots are representative of five different experiments ($n = 5$). B. The bands were quantified using densitometric analysis and data expressed as a ratio of OxyBlot band average intensity to actin band intensity. The data are means ± S.D. of five different experiments ($n = 5$). Values with shared letters are not significantly different according to Bonferroni/Dunn post hoc test.

4. Discussion

DA-loaded CS NPs were previously studied by us as a possible strategy to mask the hydrophilicity of DA in order to bypass the blood brain barrier (BBB) [1,5,14]. However, the use of a low molecular weight of CS for DA nanoencapsulation together with the supply of the antioxidant mixture GSE was never attempted before. Therefore, the design of the carrier NP was planned in order to induce a co-administration of the two agents DA and GSE, adopting a high mucoadhesive material, such as CS, whose performances for transmucosal route application are well established [26,27]. For NP formulation, an external localization of GSE was planned, thanks to the approach of the physical adsorption of the NPs onto an aqueous solution of the GSE extract. Moreover, the pH values of nanosuspensions were also measured and reported in **Table 1**, evidencing the acid pH range (3.30–4.10) due to the use of diluted acetic acid, and, consequently, further studies are required for a proper administration aiming at preventing irritation. In addition, the particle size of the investigated NPs was in the range 310–330 nm, namely higher values than mean diameters (98–148 nm) previously found by us in our previous work, where the molecular weight of the adopted CS was 110 KDa [1]. Our hypothesis is that, herein, the initial DA cargo equal to 5 mg causes size enlargement of the final NPs and such dimensional increase is also kept constant during physical adsorption of GSE. In this regard, from TEM pictures, the magnification of the NPs marked with * in **Figure 1c,d** shows an important result obtained by Cryo-TEM, namely the nanocarriers differ significantly in their surface morphology.

As can be seen from **Figure 1c** (magnification of the particle *), the NPs of CS DA TPP showed a poorly defined outer layer, probably due to the presence of residual micelles leading to the formation of a cloud-shaped surface. Interestingly, the CS DA TPP NPs ads GSE (**Figure 1d**) show a well-defined and very rough surface, characterised by the presence of small protrusions, probably due to the adsorption of GSE.

Moreover, as shown in **Table 1**, all NPs exhibited positive zeta values, although higher than the ones shown by Felice et al. [12] as a consequence of the higher molecular weight of CS, herein employed in comparison to the one cited in [12]. Precisely, when CS TPP NPs and CS DA TPP NPs were compared in terms of zeta potential, DA was argued to be on the surface of the NPs because a partial shielding of the positive charges of CS occurred, moving from +30.4 mV (i.e., CS TPP NPs) to +16.4 mV (i.e., CS DA TPP NPs, $p \leq 0.001$). Moreover, in good agreement with the zeta potential outcomes, FT-IR spectra also indicated the external localization of the

polycation CS in loaded and unloaded NPs (**Figure 3a,b**). The stretching band of C=O ascribable to CS chains detected in FT-IR spectra (**Figure 3**) allows to believe that such NPs can adhere to the extracellular mucus, so providing a useful modality for paracellular transport of active compounds [28]. In terms of active principle loading, notably, for DA containing NPs, the DA E.E.% around 50% was quite similar to the one previously found by us when glycol chitosan was the polycation forming NPs without any GSE, instead of 81% found for NPs obtained from CS having 110 KDa as molecular weight [1,5]. On the other hand, CS based NPs did not reach high E.E.% in terms of GSE (i.e., the maximum GSE E.E. value was 28%), probably due to the fact that the hydrophobicity of the phenyl rings of some compounds of GSE induces higher affinity towards the lipid Gelucire® 50/13 of the previously studied SLNs rather than towards CS [13]. However, in the case of E.E. values referring to GSE, in the presence of DA (i.e., CS DA TPP NPs ads GSE) higher E.E.% was obtained than in the case of CS TPP NPs ads GSE, maybe because non covalent interactions occurring between DA and GSE should increase the amount of the adsorbed mixture in the NPs structure. In vitro characterization included the assessment of the physical stability of the NP dispersions produced by evaluating the particle size evolution upon storage at different temperatures (**Figure 2a,b,c**). In particular, when the storage temperature was set at 37 °C by comparing CS DA TPP NPs and CS DA TPP NPs ads GSE, for the former NP aggregation was detected starting from 17 h (**Figure 2b**). For CS DA TPP NPs ads GSE, at the latest time point of incubation, the mean diameter increase was in sub-micron size range, suggesting that GSE layer adsorbed onto the NPs exerts a protective role according to a sterically stabilization mechanism that hinders reciprocal accumulation among close particles in the dispersion (**Figure 2c**). Furthermore, it could not be ruled out at all that the high value of zeta potential of CS DA TPP NPs, ads GSE also contributes to the stabilization effect towards the exposure at different temperatures. Interestingly, for both CS DA TPP NPs ads GSE and CS DA TPP NPs during storage stability studies, no change of color of the particles was optically seen, inducing to suppose that the autoxidation of DA did not occur due to different reasons, namely 1) the structural organization of NPs (for CS DA TPP NPs); 2) the adsorbed GSE layer for CS DA TPP NPs ads GSE, able to exert its antioxidant role towards the early degradation of the neurotransmitter. In principle, colloidal aggregation could be induced by several factors as already discussed, but, on the base of the biological results, the aggregation process occurring at 37 °C did not hinder the performance of the NPs containing DA and/or GSE [29]. In this regard, in the present work SHSY-5Y cells were selected because, being widely used to study pathogenesis, this cell line expresses such representative dopaminergic markers as tyrosine hydroxylase and dopamine transporter which are relevant for investigations concerning PD [30,31]. **Figure 5** elucidates that DA accumulation in SHSY-5Y cells occurred in both types of NPs thanks to the vectorization of the CS-based nanoparticulate system. It was an interesting finding considering that the hydrophilic features of DA are well known to be unfavorable to the BBB crossing, so limiting its therapeutic efficacy. Moreover, SHSY-5Y cells also represented a suitable model system to study the role of CS DA TPP NPs ads GSE NPs against ROS-mediated dopaminergic cell death and, herein, the protective effects of CS DA TPP NPs ads GSE NPs are

ascribable to the suppression of ROS generation (**Figure 4b**). Such preventive capacity is very effective than that induced by other natural compounds in the same DA-treated SHSY-5Y cell line, such as is borneol, pyrroloquinoline quinone and baicalein [32–34].

In the literature, DA-induced neuronal apoptosis has been suggested to be mediated by ROS generation and mitochondrial dysfunction, common events leading to neuronal apoptosis in PD [35]. On the other hand, although some antioxidant compounds possess neuroprotective effects in PD, the lack of efficacy to penetrate the BBB led them to fail in in vivo effects. Maybe the strategy of nanoparticle administration seems to be encouraging and, hence, providing both DA and GSE which in a synergic manner are required in the neurological disorder of PD.

Furthermore, the cytoprotective ability of CS DA TPP NPs ads GSE NPs, and CS TPP NPs ads GSE NPs can be deduced thanks to the inhibitory effect exerted towards DA-induced stress according to OxyBlot results shown in **Figure 6**. Some examples of OxyBlot application to investigations concerning PD and Alzheimer's disease (AD) have been previously reported [36–38]. In a rat model of AD, brain tissue analyses showed that deferoxamine treatment decreased oxidation as measured by OxyBlot [37]. In the case of autosomal recessive PD, the oxidative stress related to Parkin mutations in a human cellular model was also investigated by OxyBlot [38].

To the best of our knowledge, this is the first work where OxyBlot test was adopted for measuring oxidative stress in the presence of chitosan nanoparticles and the resulting protection exerted by the antioxidant mixture GSE induces us to plan further studies which can better address the application of such NPs for PD treatment.

5. Conclusions

In the last decades, polyphenols received special attention due to their nutraceutical and pharmacological activities for the prevention and treatment of some diseases. Nevertheless, their photosensitivity and low bioavailability are some drawbacks which could limit their application. In this work, a new nanostructured carrier consisting of low molecular weight CS, DA, and polyphenol enriched GSE was described as a candidate formulation for PD application. High percentages of encapsulation efficiency of DA and GSE were found in the NPs and multiple biological assays evidenced good tolerability of the NPs in SHSY-5Y cell model line. Overall, the possible cooperation role occurring between DA and GSE administered by NPs was herein envisaged and future research work will better clarify how such NPs can be addressed to obtain a suitable pharmaceutical dosage form for PD treatment.

Author contributions: Conceptualization, SB and AT; methodology, AT and GF; software, AC and DD; validation, AT, LC, FC and AP; investigation, AT, DEM, AM, SM, ES and LC; resources, AT; writing—original draft preparation, AT, SM and AM; writing—review and editing, AT, SM and AM; supervision, AT, SB and GF; funding acquisition, AT. All authors have read and agreed to the published version of the manuscript.

Funding: This research was funded by Horizon-Europeseeds (Project NAMOPARCHIP-CUP H99J21017020006)-University of Bari "Aldo Moro" (Italy).

Acknowledgments: Giuseppe Fracchiolla, Filomena Corbo and Adriana Trapani would acknowledge Mr. Sergio Cellamare and Mr. Giovanni Dipinto (University of Bari, Italy) for their valuable technical assistance.

Data availability statement: Data are available by the corresponding authors.

Conflict of interest: The authors declare no conflict of interest.

References

1. Trapani A, De Giglio E, Cafagna D, et al. Characterization and evaluation of chitosan nanoparticles for dopamine brain delivery. International Journal of Pharmaceutics 2011; 419(1-2): 296–307. doi: 10.1016/j.ijpharm.2011.07.036.
2. Aktas Y, Andrieux K, Alonso MJ, et al. Preparation and in vitro evaluation of chitosan nanoparticles containing a caspase inhibitor. International Journal of Pharmaceutics 2005; 298(2): 378–383. doi: 10.1016/j.ijpharm.2005.03.027.
3. Calvo P, Remunan-Lopez C, Vila-Jato JL, Alonso MJ. Novel hydrophilic chitosan-polyethylene oxide nanoparticles as protein carrier. Journal of Applied Polymer Science 1997; 63(1): 125–132. doi: 10.1002/(SICI)1097-4628(19970103)63:1<125::AID-APP13>3.0.CO;2-4.
4. Tobio M, Sánchez A, Vila A, et al. The role of PEG on the stability in digestive fluids and in vivo fate of PEG-PLA nanoparticles following oral administration. Colloids and Surfaces B: Biointerfaces 2000; 18(3-4): 315–323. doi: 10.1016/S0927-7765(99)00157-5.
5. Di Gioia S, Trapani A, Mandracchia D, et al. Intranasal delivery of dopamine to the striatum using glycol chitosan/sulfobutylether-β-cy- clodextrin based nanoparticles. European Journal of Pharmaceutics and Biopharmaceutics 2015; 94: 180–193. doi: 10.1016/j.ejpb.2015.05.019.
6. Conese M, Cassano R, Gavini E, et al. Harnessing stem cells and neurotrophic factors with novel technologies in the treatment of Parkinson's disease. Current Stem Cell Research & Therapy 2019; 14(7): 549–569. doi: 10.2174/1574888X14666190301150210.
7. Rocha EM, De Miranda B, Sanders LH. Alpha-synuclein: Pathology, mitochondrial dysfunction and neuroinflammation in Parkinson's disease. Neurobiology of Disease 2018; 109(Pt B): 249–257. doi: 10.1016/j.nbd.2017.04.004.
8. Zemljič LF, Plohl O, Vesel A, et al. Physicochemical characterization of packaging foils coated by chitosan and polyphenols colloidal formulations. International Journal of Molecular Sciences 2020; 21(2): 495. doi: 10.3390/ijms21020495.
9. Fahmy HM, Khadrawy YA, Abd-El Daim TM, et al. Thymoquinone-encapsulated chitosan nanoparticles coated with polysorbate 80 as a novel treatment agent in a reserpine-induced depression animal model. Physiology & Behavior 2020; 222: 112934. doi: 10.1016/j.physbeh.2020.112934.
10. Md S, Alhakamy NA, Aldawsari HM, Asfour HZ. Neuroprotective and antioxidant effect of naringenin-loaded nanoparticles for nose-to-brain delivery. Brain Sciences 2019; 9(10): 275. doi: 10.3390/brainsci9100275.
11. Ahlawat J, Neupane R, Deemer E, et al. Chitosan-ellagic acid nanohybrid for mitigating rotenone-induced oxidative stress. ACS Applied Materials & Interfaces 2020; 12(16): 18964–18977. doi: 10.1021/acsami.9b21215.
12. Felice F, Zambito Y, Belardinelli E, et al. Delivery of natural polyphenols by polymeric nanoparticles improves the resistance of endothelial progenitor cells to oxidative stress. European Journal of Pharmaceutical Sciences 2013; 50(3-4): 393–399. doi: 10.1016/j.ejps.2013.08.008.
13. Trapani A, Guerra L, Corbo F, et al. Cyto/Biocompatibility of dopamine combined with the antioxidant grape seed-derived polyphenol compounds in solid lipid nanoparticles. Molecules 2021; 26(4): 916. doi: 10.3390/molecules26040916.
14. De Giglio E, Trapani A, Cafagna D, et al. Dopamine-loaded chitosan nanoparticles: Formulation and analytical characterization. Analytical and Bioanalytical Chemistry 2011; 400: 1997–2002. doi: 10.1007/s00216-011-4962-y.
15. Castellani S, Trapani A, Spagnoletta A, et al. Nanoparticle delivery of grape seed-derived proanthocyanidins to airway epithelial cells dampens oxidative stress and inflammation. Journal of Translational Medicine 2018; 16(1): 140. doi: 10.1186/s12967-018-1509-4.
16. Trapani A, Esteban MÁ, Curci F, et al. Solid lipid nanoparticles administering antioxidant grape seed-derived polyphenol compounds: A potential application in aquaculture. Molecules 2022; 27(2): 344. doi: 10.3390/molecules27020344.

17. Trapani A, De Giglio E, Cometa S, et al. Dopamine-loaded lipid based nanocarriers for intranasal administration of the neurotransmitter: A comparative study. European Journal of Pharmaceutics and Biopharmaceutics 2021; 167: 189–200. doi: 10.1016/j.ejpb.2021.07.015.
18. Cometa S, Bonifacio MA, Trapani G, et al. In vitro investigations on dopamine loaded Solid Lipid Nanoparticles. Journal of Pharmaceutical and Biomedical Analysis 2020; 185: 113257. doi: 10.1016/j.jpba.2020.113257.
19. Carbone C, Campisi A, Manno D, et al. The critical role of didodecyldimethylammonium bromide on physico-chemical, technological and biological properties of NLC. Colloids and Surfaces B: Biointerfaces 2014; 121: 1–10. doi: 10.1016/j.colsurfb.2014.05.024.
20. Mandracchia D, Trapani A, Perteghella S, et al. pH-sensitive inulin-based nanomicelles for intestinal site-specific and controlled release of celecoxib. Carbohydrate Polymers 2018; 181: 570–578. doi: 10.1016/j.carbpol.2017.11.110.
21. Di Gioia S, Trapani A, Cassano R, et al. Nose-to-brain delivery: A comparative study between carboxymethyl chitosan based conjugates of dopamine. International Journal of Pharmaceutics 2021; 599: 120453. doi: 10.1016/j.ijpharm.2021.120453.
22. Trapani A, De Laurentis N, Armenise D, et al. Enhanced solubility and antibacterial activity of lipophilic fluoro-substituted N-benzoyl-2-aminobenzothiazoles by complexation with β-cyclodextrins. International Journal of Pharmaceutics 2016; 497(1-2): 18–22. doi: 10.1016/j.ijpharm.2015.11.024.
23. Trapani A, Catalano A, Carocci A, et al. Effect of Methyl-β-Cyclodextrin on the antimicrobial activity of a new series of poorly water-soluble benzothiazoles. Carbohydrate Polymers 2019; 2017: 720–728. doi: 10.1016/j.carbpol.2018.12.016.
24. Oliveira HR, Verlengia R, Carvalho CRO, et al. Pancreatic beta-cells express phagocyte-like NAD(P)H oxidase. Diabetes 2003; 52(6): 1457–1463. doi: 10.2337/diabetes.52.6.1457.
25. Wang SF, Yen JC, Yin PH, et al. Involvement of oxidative stress-activated JNK signaling in the methamphetamine-induced cell death of human SH-SY5Y cells. Toxicology 2008; 246(2-3): 234–241. doi: 10.1016/j.tox.2008.01.020.
26. Raj R, Wairkar S, Sridhar V, Gaud R. Pramipexole dihydrochloride loaded chitosan nanoparticles for nose to brain delivery: Development, characterization and in vivo anti-Parkinson activity. International Journal of Biological Macromolecules 2018; 109: 27–35. doi: 10.1016/j.ijbiomac.2017.12.056.
27. Mistry A, Glud SZ, Kjems J, et al. Effect of physicochemical properties on intranasal nanoparticle transit into murine olfactory epithelium. Journal of Drug Targeting 2009; 17(7): 543–552. doi: 10.1080/10611860903055470.
28. Rukmangathen R, Yallamalli IM, Yalavarthi PR. Biopharmaceutical potential of selegiline loaded chitosan nanoparticles in the management of Parkinson's disease. Current Drug Discovery Technologies 2019; 16(4): 417–425. doi: 10.2174/1570163815666180418144019.
29. Santander-Ortega MJ, Jódar-Reyes AB, Csaba N, et al. Colloidal stability of pluronic F68-coated PLGA nanoparticles: A variety of stabilisation mechanisms. Journal of Colloid and Interface Science 2006; 302(2): 522–529. doi: 10.1016/j.jcis.2006.07.031.
30. Hasegawa T, Matsuzaki M, Takeda A, et al. Increased dopamine and its metabolites in SH-SY5Y neuroblastoma cells that express tyrosinase. Journal of Neurochemistry 2003; 87(2): 470–475. doi: 10.1046/j.1471-4159.2003.02008.x.
31. Chatzitaki AT, Jesus S, Karavasili C, et al. Chitosan-coated PLGA nanoparticles for the nasal delivery of ropinirole hydrochloride: In vitro and ex vivo evaluation of efficacy and safety. International Journal of Pharmaceutics 2020; 589: 119776. doi: 10.1016/j.ijpharm.2020.119776.
32. Tian L, Zhou Z, Zhang Q, et al. Protective effect of (±) isoborneol against 6-OHDA-induced apoptosis in SH-SY5Y cells. Cellular Physiology and Biochemistry 2007; 20(6): 1019–1032. doi: 10.1159/000110682.
33. Hara H, Hiramatsu H, Adachi T. Pyrroloquinoline quinone is a potent neuroprotective nutrient against 6-hydroxydopamine-induced neurotoxicity. Neurochemical Research 2007; 32: 489–495. doi: 10.1007/s11064-006-9257-x.
34. Lee HJ, Noh YH, Lee DY, et al. Baicalein attenuates 6-hydroxydopamine-induced neurotoxicity in SH-SY5Y cells. European Journal of Cell Biology 2005; 84(11): 897–905. doi: 10.1016/j.ejcb.2005.07.003.
35. Foster KA, Galeffi F, Gerich FJ, et al. Optical and pharmacological tools to investigate the role of mitochondria during oxidative stress and neurodegeneration. Progress in Neurobiology 2006; 79(3): 136–171. doi: 10.1016/j.pneurobio.2006.07.001.
36. Terracciano C, Nogalska A, Engel WK, et al. In inclusion-body myositis muscle fibers Parkinson-associated DJ-1 is increased and oxidized. Free Radical Biology & Medicine 2008; 45(6): 773–779. doi: 10.1016/j.freeradbiomed.2008.05.030.

37. Fine JM, Forsberg AC, Stroebel BM, et al. Intranasal deferoxamine affects memory loss, oxidation, and the insulin pathway in the streptozotocin rat model of Alzheimer's disease. Journal of the Neurological Sciences 2017; 380: 164–171. doi: 10.1016/j.jns.2017.07.028.
38. Grünewald A, Voges L, Rakovic A, et al. Mutant Parkin impairs mitochondrial function and morphology in human fibroblasts. PLoS One 2010; 5(9): e12962. doi: 10.1371/journal.pone.0012962.